Available online at www.sciencedirect.com
ScienceDirect
Geochimica et Cosmochimica Acta 70 (2006) 6118–6135
Geochimica
www.elsevier.com/locate/gca

Sulfates on Mars: A systematic Raman spectroscopic study of hydration states of magnesium sulfates

Alian Wang [a,*], John J. Freeman [a], Bradley L. Jolliff [a], I-Ming Chou [b]

[a] Department of Earth and Planetary Sciences and McDonnell Center for Space Sciences, Washington University, St. Louis, MO 63130, USA
[b] U.S. Geological Survey, 954 National Center, Reston, VA 20192, USA

Received 7 February 2006; accepted in revised form 31 May 2006

Abstract

The martian orbital and landed surface missions, OMEGA on Mar Express and the two Mars Explorations Rovers, respectively, have yielded evidence pointing to the presence of magnesium sulfates on the martian surface. *In situ* identification of the hydration states of magnesium sulfates, as well as the hydration states of other Ca- and Fe- sulfates, will be crucial in future landed missions on Mars in order to advance our knowledge of the hydrologic history of Mars as well as the potential for hosting life on Mars. Raman spectroscopy is a technique well-suited for landed missions on the martian surface. In this paper, we report a systematic study of the Raman spectra of the hydrates of magnesium sulfate. Characteristic and distinct Raman spectral patterns were observed for each of the 11 distinct hydrates of magnesium sulfates, crystalline and non-crystalline. The unique Raman spectral features along with the general tendency of the shift of the position of the sulfate v_1 band towards higher wavenumbers with a decrease in the degree of hydration allow *in situ* identification of these hydrated magnesium sulfates from the raw Raman spectra of mixtures. Using these Raman spectral features, we have started the study of the stability field of hydrated magnesium sulfates and the pathways of their transformations at various temperature and relative humidity conditions. In particular we report on the Raman spectrum of an amorphous hydrate of magnesium sulfate ($MgSO_4{\cdot}2H_2O$) that may have specific relevance for the martian surface.

1. Introduction

The sulfur enrichment and the compositional correlations of Mg and S within martian surface materials were first found in X-ray fluorescence data during Viking missions (Clark et al., 1982). Both observations were confirmed by the APXS (Alpha Particle X-ray Spectrometer) experiments on the Sojourner rover of the Mars Pathfinder mission (Rieder et al., 1997; McSween et al., 1999) and on the Spirit and the Opportunity rovers of the Mars Exploration Rovers (MER) missions (Gellert et al., 2004, 2006; Rieder et al., 2004). The correlations between Ca and S, and Fe and S have also been found in various regions at the Gusev landing site (Haskin et al., 2005; Ming et al., 2006; Wang et al., 2006a). Chemical correlations from these landed missions imply that sulfate salts are important constituents in martian surface and subsurface materials. There is only one direct identification of sulfate, as a mineral, from the landed missions on Mars, jarosite [$KFe^{3+}(SO_4)_2(OH)_6$], which was identified through Mössbauer spectrometer analysis (Klingelhöfer et al., 2004) by the Opportunity rover at Meridiani Planum.

By comparison, a variety of sulfates has been identified through the results of the Mars Express orbital mission. The OMEGA spectrometer (Observatiore pour la Minéralogie, l'Eau, les Glacies, et l'Activitié) observed characteristic near infrared (NIR) peaks of sulfates at various locations on Mars (Bibring et al., 2005), including Meridiani Planum where the Opportunity rover landed (Arvidson et al., 2005). The types of sulfates definitively identified from OMEGA spectra were kieserite ($MgSO_4{\cdot}H_2O$), gypsum ($CaSO_4{\cdot}2H_2O$), and bassanite ($2CaSO_4{\cdot}H_2O$). Another

* Corresponding author. Fax: +1 314 935 7361.
E-mail address: alianw@levee.wustl.edu (A. Wang).

0016-7037/$ - see front matter © 2006 Elsevier Inc. All rights reserved.
doi:10.1016/j.gca.2006.05.022

type of OMEGA spectrum was assigned to polyhydrated sulfates and the sulfates with different cations, for which the spectra of epsomite ($MgSO_4{\cdot}7H_2O$), copiapite ($Fe^{2+}Fe^{3+}{}_4(SO_4)_6(OH)_2 \cdot 20H_2O$), and halotrichite ($Fe^{2+}Al_2(SO_4)_4{\cdot}22H_2O$) would provide matches (Gendrin et al., 2005). A few percent of adsorbed water was also assigned on the basis of observations that (1) 3 μm absorption bands are observed in every spectrum obtained by OMEGA; and (2) the 3-μm band intensity is positively correlated with the high albedo areas on Mars.

The neutron spectrometer (NS) component of the gamma-ray spectrometer suite (GRS) on board the Mars Odyssey spacecraft detected high concentrations of hydrogen in two broad equatorial regions in the neighborhood of Arabia Terra (centered at −5°N, +25°E) and Medusae Fossae (centered at −15°N, +180°E), which cover respectively the Meridiani Planum and Gusev Crater sites (Boynton et al., 2002; Feldman et al., 2004). The relative maxima in hydrogen abundances correlate topographically with mid- and low-altitude areas. Because water–ice should not be stable under the current conditions at the surface and near surface of these equatorial areas, the hydrogen is assumed to reside in hydrated minerals although ground ice cannot totally be ruled out (Boynton et al., 2002; Feldman et al., 2004, 2005).

Mars apparently had large amounts of surface water in the past that could plausibly have produced evaporite deposits, including water-bearing minerals such as the hydrated sulfates (Carr, 1996; Hynek and Phillips, 2001, 2003; Carr and Head, 2003; Squyres et al., 2004).

Sulfur-bearing materials associated with the sulfur cycle must have played an important role in the evolution and hydrologic history of Mars. Large amounts of sulfur may have originated from volcanic outgassing, in the form of H_2S or SO_2, which could react with oxidizing atmospheric components to form $[SO_3]^{2-}$, $[HSO_4]^{-}$, or $[H_2SO_4]$, and then fall onto the martian surface. During a warm and wet era, these gaseous species would have dissolved in water to form acidic aqueous solutions. The solutions would be neutralized by reacting with igneous minerals, which release Mg, Ca, Fe, and Al cations. At high degrees of alteration, sulfides, as minor phases in igneous mineral assemblages (as seen in martian meteorites), would also be oxidized and S released into solution.

Sulfur-rich solutions might also originate from hydrothermal alteration associated with convection cells driven by intrusive igneous activity, especially in areas near long-lived volcanic provinces. Igneous activity would have occurred throughout Noachian time and may have extended to geologically recent times, judging from relatively young ages of some of the martian basaltic meteorites. Such solutions might also be mixed and carried laterally by surface or ground waters, and eventually deposited in evaporite sulfates. Sulfur-bearing phases at different stages of the cycle and phase transitions among them would provide energy sources for metabolic processes of bio-species, as seen on Earth (Tosca et al., 2004; Golden et al., 2005).

Planetary Raman spectroscopy is a powerful tool for *in situ* identification of minerals and biogenic species expected (potentially) to be encountered in planetary surface exploration (Wdowiak et al., 1994; Wang et al., 1995; Haskin et al., 1997; Wynn-Williams and Edwards, 2000). A laser Raman spectroscopy (LRS) experiment can characterize, structurally and compositionally, many classes of minerals and inorganic compounds such as silicates, carbonates, sulfates, phosphates, oxides, sulfides, and oxyhydroxides, as well as clathrates of CO_2 and CH_4. Additionally, Raman spectroscopy is useful for characterizing the organic species produced in biogenic or non-biogenic processes where it can distinguish functional groups in organics materials containing H–O, H–N, H–C, N–O, C–O, C–N, and P–O bonds (Nakamoto, 1997). All species in the sulfur cycle on Earth have a diagnostic Raman spectrum that would enable *in situ* identification. A Raman instrument suitable for martian surface studies is the Mars Microbeam Raman Spectrometer (MMRS) that we have developed which combines a microbeam Raman detection capability with a line-scanning capability (Haskin et al., 1997; Wang et al., 1998, 2003). This system permits trace constituents in a target to be detected (Wang et al., 2004b) in addition to the major and minor phases. The line scanning capability of the MMRS can be used to obtain information on the distributions and relative proportions of species and on grain sizes and the rock textures (Wang et al., 1999a); thus, the mineralogical information can be correlated directly with morphological microscopic imaging (Wang et al., 1999b; Kuebler et al., 2003). In addition, remote Raman technology has been developed in recent years, which shows the effective detections of various mineral phases from a distance of ~10 m (Sharma et al., 2002; Misra et al., 2006).

Among all species involved in S-cycling, hydrated sulfate minerals bear special interest due to the recent discoveries by the Mars Exploration Rover missions and Mars Express OMEGA. There is no systematic Raman spectroscopic study to date in the literature on the full range of hydrated magnesium and iron sulfates (LaFont and Vinh, 1966; Chio et al., 2004, 2005; Wang et al., 2005; Sharma et al., 2006). We report in this paper, our first study of Raman experiments on the full range of hydrated Mg-sulfates.

2. Importance of studying the hydration states of sulfates

The highest concentration of Mg-sulfates found by the Spirit rover (inferred from the APXS data) at Gusev thus far has been in the subsurface regolith at The Boroughs trench (Wang et al., 2005b; Wang et al., 2006a). The distribution of sulfates in subsurface regolith within this trench is heterogeneous. By first-order approximation, sulfates make about 22 wt% of subsurface regolith at the most sulfur-rich spot in the trench, and approximately 85 mole % of these sulfates consists of Mg-sulfate. Assuming all these Mg-sulfates are in the form of kieserite as seen by OMEGA from other locations on Mars including Meridiani Planum,

Table 1
Estimates of water content based on mixing-model analyses on two targets at Gusev Crater. (a) The Borough trench regolith which shows a positive Mg vs. SO_4 correlation and for which mixing-model analysis suggests a maximum of ~22 wt% sulfates

Water-bearing phases (assumed hydration state of Mg-sulfates)	Corresponding wt% of water in regolith at		
	Trench wall	Trench floor	Subsurface
$MgSO_4 \cdot H_2O$, Kieserite[a]	**3.1**	**2.5**	**1.0**
$MgSO_4 \cdot 2H_2O$, Sanderite	6.0	4.8	2.1
$MgSO_4 \cdot 3H_2O$	8.7	7.0	3.1
$MgSO_4 \cdot 4H_2O$, Starkeyite	11.3	9.2	4.0
$MgSO_4 \cdot 5H_2O$, Pentahydrite	13.7	11.2	5.0
$MgSO_4 \cdot 6H_2O$, Hexahydrite	16.0	13.2	5.9
$MgSO_4 \cdot 7H_2O$, Epsomite	18.2	15.0	6.9

(b) Wooly Patch outcrop, which shows a positive Ca vs. SO_4 correlation and an excess of Si and Al, and for which mixing-model analysis suggests the presence of Ca- and Mg-sulfates (72.5:27.5) and kaolinite-type phyllosilicates

Water-bearing phases (assumed hydration states of Ca- and Mg-sulfate)	Corresponding wt% of water in outcrop	
	Mastodon target	Sabre target
$MgSO_4 \cdot H_2O$, $CaSO_4$, kaolinite	2.1	2.6
$MgSO_4 \cdot H_2O$, $CaSO_4 \cdot 0.5H_2O$, kaolinite	2.2	2.8
$MgSO_4 \cdot H_2O$, $CaSO_4 \cdot 2H_2O$, kaolinite	**2.8**	**3.5**
$MgSO_4 \cdot 4H_2O$, $CaSO_4 \cdot 2H_2O$, kaolinite	3.2	4.0
$MgSO_4 \cdot 7H_2O$, $CaSO_4 \cdot 2H_2O$, kaolinite	3.7	4.5

the water held by these kieserite molecules would make ~3 wt% of the regolith (Table 1a).

Phyllosilicates are suggested as potential constituents in some rocks in the Columbia Hills at Gusev Crater, judging by the distinct compositional features of these rocks (Wang et al., 2005a, 2006b; Clark et al., 2005). These phyllosilicates, kaolinite or montmorillonite, coexist with sulfates and unaltered igneous minerals. On the basis of Ca and S correlations found in West Spur rocks (Wang et al., 2006b) in the Columbia Hills, we could assume gypsum is the major form of Ca-sulfates and kieserite is the major form of Mg-sulfates. On the basis of these assumptions, the total water concentration held by sulfates and phyllosilicates in the rock "Wooly Patch" on West Spur at Gusev could be ~3 wt% of the whole rock (Table 1b).

A much higher water-equivalent-hydrogen (WEH) value, however, is indicated by the NS–GRS (neutron spectrometer in gamma-ray spectrometer suite) of the Mars Odyssey mission in the vicinity of Gusev Crater (Feldman et al., 2005). Using the epithermal-neutron data, an average WEH concentration of ~7 wt% was found over a footprint of 600 km diameter, which covers the entire Gusev Crater, its in-flow channel Ma'Adim Valles, and the lowlands around Gusev Crater and Apollinaris Patera (Fig. 1). When using these assumptions on hydration states for sulfates (i.e., gypsum for Ca-sulfates and kieserite for Mg-sulfates), and averaging the potential water held by all the rock and soil targets at Gusev investigated by the Spirit rover thus far, the water concentration value would be <1 wt%. Even adding a few percent for the water potentially adsorbed in the interstitial spaces among soil grains and surface dust particles, the water content would be much lower than the WEH value inferred from the NS–GRS.

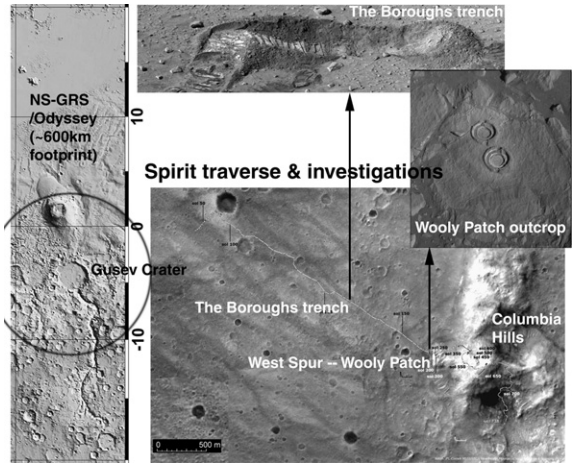

Fig. 1. Spatial correlations among orbital observations and surface exploration at Gusev Crater (http://ltpwww.gsfc.nasa.gov/tharsis/Mars_topography_from_MOLA/; other images from Wang et al., 2006a,b).

This discrepancy suggests additional water reservoirs in the vicinity of Gusev Crater. We consider two possibilities: one, that ground ice or other types of water-rich entities (e.g., evaporite deposits) occur at locations where Spirit has not yet explored; another is that Mg-sulfate minerals in the subsurface regolith actually hold more water by maintaining hydration states higher than kieserite.

In order to improve our understanding of Mars surface mineralogy and geochemistry based on the data from these missions and to address the hydrologic history of Mars, it is crucial to improve knowledge of the stability field of various hydrated sulfates under martian conditions (past and

present), and the pathways and the rates of phase transformations. These data will also help to provide insight to the geochemical processes and evolution during the diurnal cycle, the obliquity cycles, and throughout martian geological time during which the surface has been modified by volcanic, impact, aqueous, and eolian processes.

Several studies concerning the hydrated sulfates have been published in the past few years. Among them, Vaniman et al. (2004, 2005) reported that structurally amorphous Mg-sulfates can be formed rapidly (in a few hours or a day) from hexahydrite ($MgSO_4{\cdot}6H_2O$) under low relative humidity (0.3–0.4% RH) or with a vacuum at 1 torr (132 Pa) total pressure. They suggest the number of structural waters held by this amorphous phase can vary from 2 to 1.2. Because of the large relative-humidity swing during the current diurnal cycle on the surface of Mars, varying from <1% RH (~290 K) at mid-day summer to near 100% RH (~180 K) during the cold early morning, kieserite at the surface would convert to hexahydrite (and epsomite) at high RH and then dehydrate to form hydrated amorphous Mg-sulfate, whose re-hydration is extremely sluggish at night-time temperatures. Therefore, the hydrated amorphous phase, not kieserite, would be the favored Mg-sulfate at the martian surface today.

Chipera et al. (2005) demonstrated that besides hexahydrite and epsomite, other hydrated phases of Mg-sulfate, especially starkeyite ($MgSO_4{\cdot}4H_2O$), can be stable and co-exist with kieserite under martian surface conditions. The phase transformations between these different hydrated phases of Mg-sulfates are characterized by sluggish kinetics, path dependence, and the presence of metastable intermediate states of hydration.

Chou and Seal determined the epsomite–hexahydrite equilibria (Chou and Seal, 2003) and starkeyite–hexahydrite equilibria (Chou et al., 2005) as a function of both temperature and relative humidity using the humidity-buffer technique. Their results suggest that kieserite, starkeyite, epsomite, and $MgSO_4{\cdot}12H_2O$ (based on a recent work by Peterson and Wang, 2006, we will use $MgSO_4{\cdot}11H_2O$ to represent this phase) would be the possible crystalline Mg-sulfate phases existing under current conditions in martian regolith in equatorial regions.

On the basis of the work of Vaniman et al. (2004, 2005), Chipera et al. (2005), Chou and Seal (2003) and Chou et al. (2005), the de-hydration and re-hydration of Mg-sulfates in martian regolith could occur within hours during every martian sol. In this paper, we report first that all 11 types of known anhydrous and hydrous forms of magnesium sulfates have diagnostic Raman spectral patterns that can be used to identify them from raw spectra of mixtures. We then discuss how these Raman features enable us to study the stability and meta-stability fields of the hydrated phases, to characterize the hydrated amorphous phases, and to monitor the phase-transformation pathways under changing environmental conditions.

3. Sample preparations and measurements

We list in Table 2 the anhydrous and hydrated phases of Mg-sulfate that we have investigated in this study. We purchased commercially available anhydrous β-$MgSO_4$ (Sigma–Aldrich, ReagentPlus™, >99%, Batch 025K0154), $MgSO_4{\cdot}H_2O$ (Sigma–Aldrich, >97%, Batch 12426BC), and $MgSO_4{\cdot}7H_2O$ (Sigma–Aldrich, SigmaUltra, ⩾98%, Batch 084k01061) as starting materials. We used four types of preparations to produce other hydration states of Mg-sulfate. Laser Raman spectroscopy (LRS) and X-ray diffraction (XRD) measurements were used to characterize the starting materials and the reaction products. The masses of samples were measured before and after reactions to monitor the variations in hydration states in the de-hydration and re-hydration experiments.

Table 2
Past and current Raman and XRD studies of hydrous and anhydrous Mg-sulfates

Chemical formula	Crystal structure	Space group	XRD std data	Raman study in literature	This Raman study
Aqueous $[SO_4]^{2-}$	In solution		No	g	Yes
$MgSO_4{\cdot}11H_2O$	Triclinic	$P\bar{1}-C_i^1$	i	No	Yes
$MgSO_4{\cdot}7H_2O$	Orthorhombic	$P2_12_12_1-D_2^4$	a	h	Yes
$MgSO_4{\cdot}6H_2O$	Monoclinic	$C2/c-C_{2h}^6$	b	h	Yes
$MgSO_4{\cdot}5H_2O$	Triclinic	$P\bar{1}-C_i^1$	c	No	Yes
$MgSO_4{\cdot}4H_2O$	Monoclinic	$P2_1/b-C_{2h}^5$	d	No	Yes
$MgSO_4{\cdot}3H_2O$	Unknown	Unknown	Yes	No	Yes
$MgSO_4{\cdot}2H_2O$	Monoclinic	Unknown	Yes	No	Yes
$MgSO_4{\cdot}1.2–2H_2O$	Non-crystalline		No	No	Yes
$MgSO_4{\cdot}H_2O$	Monoclinic	$C2/c-C_{2h}^6$	e	No	Yes
β-$MgSO_4$	Orthorhombic	$Cmcm-D_{2h}^{17}$	f	No	Yes

a. Baur (1964a).
b. Zalkin et al. (1964).
c. Baur and Rolin (1972).
d. Baur (1964b).
e. Aleksovska (1998).
f. Rentzeperis and Soldatos (1958).
g. Zangmeister and Pemberton (2000).
h. LaFont and Vinh (1966).
i. Peterson and Wang (2006).

3.1. Direct crystallization from saturated solutions

The methods we used are based on those described by Emons et al. (1990) and involve crystallization from saturated $MgSO_4$ solution, oversaturated methanolic $MgSO_4$ solution, and mixtures of saturated $MgSO_4$ and $MgCl_2$ solutions. Pure epsomite and hexahydrite were produced. From the preparations targeted on Mg-sulfates with 2–5 structural water molecules, however, we only obtained mixtures of Mg-sulfates with various hydration states. Nevertheless, using Raman microbeam analysis, single-phase Raman spectra of most hydration states of the Mg-sulfates were obtained from individual crystals within these mixtures. The assignments of these Raman spectra were later confirmed by coupled LRS and XRD measurements on the pure samples prepared using two other methods.

3.2. Heating solid samples at fixed temperatures

Baking epsomite at different temperatures in an open oven has produced homogenous kieserite (at 95 °C) and starkeyite (at 40 °C) samples, with sufficient quantities for XRD verification of LRS spectral assignments. The temperature of the oven was held at the set point to within ±1 °C, whereas the water-vapor pressure in the oven was determined by the relative humidity of the laboratory which varied from 30% to 55% RH depending on the season.

3.3. Vacuum desiccation of solid samples

A vacuum desiccator kept at room temperature (21 ± 1 °C) was used to convert epsomite and hexahydrite into amorphous $MgSO_4$, which was reported in the experiments of Vaniman et al. (2004, 2005). The vacuum in the desiccator was kept at about 0.5 torr (~67 Pa) for two experiments of 5 and 15 days duration. LRS and XRD measurements were made on the samples in sealed containers immediately after removal from the vacuum.

3.4. Using humidity buffer solutions to convert the hydration states

We used the humidity-buffer technique (Chou et al., 2002) to convert the magnesium sulfates of different hydration states at fixed temperature (T) and relative humidity (RH) conditions. The humidity-buffers we used are based on saturated aqueous solutions of the binary salts, LiBr, LiCl, $MgCl_2$, $Mg(NO_3)_2$, NaBr, KI, NaCl, KCl, KNO_3, as well as pure water (Chou et al., 2002; Greenspan, 1977). Humidity-buffer solutions were contained in 60 mm diameter straight-wall, capped glass bottles. Solutions were prepared from 25 ml of water plus sufficient salt to produce a saturated solution with excess salt. A thin layer of powdered starting Mg-sulfate (~0.2 g, ground and sieved with a grain-size range of <75 μm) was placed at the bottom of a 30 mm diameter, straight-wall Kimax® glass reaction vial. This vial was selected because it is free of laser-induced fluorescence and has a size that can be mounted on the microscopic stage of the LRS system. The uncapped reaction vial was placed upright in the tightly capped solution bottle. For each type of starting Mg-sulfate, a set of de-hydration and re-hydration experiments was conducted using a full range of humidity buffer solutions at constant temperatures, either in the oven at 50 ± 1 °C, or in the laboratory at 21 ± 1 °C. An epsomite reaction vial was kept over a 100% RH buffer within an isolated freezer compartment of a laboratory refrigerator at −5 °C to produce $MgSO_4{\cdot}11H_2O$. This experimental procedure allows free interaction of the fine Mg-sulfate grains with water vapor at pre-determined RH and T. The Mg-sulfate samples were allowed to equilibrate in the humidity buffer bottles for weeks and in some cases several months. We monitored the progress of the de-hydration/re-hydration experiments by measuring the mass of the reaction vial (capped immediately after its removal from the humidity buffer bottle), and by measuring the Raman spectra of the intermediate products through the glass wall of the sealed reaction vials. The LRS measurements took only minutes to complete and were made at regular time intervals throughout the entire de-hydration/re-hydration process. The final products were measured with both LRS and XRD techniques.

3.5. XRD measurements

A Rigaku Geigerflex X-ray diffractometer with a CuKα radiation source was used in this study. Data reduction was done using the Jade™ software. The protocol for XRD measurements of unstable Mg-sulfate samples was to first collect the Raman spectrum of the sample with the sample still in its sealed glass vial. Then about 0.2–0.3 g of sample were quickly ground together with CaF_2 powder as an internal standard and immediately sealed in the well of an XRD powder sample holder using an extremely thin plastic film (Saran Wrap®). At the end of the XRD pattern collection, the Raman spectrum of the sample, still in the sealed XRD sample holder, was collected again. The powdered CaF_2 added to the Mg-sulfate samples provides two strong diffraction lines as the internal standard for calibration of the XRD system. The plastic film covering the samples produces one strong line at 21.3°2θ and a few weak features (20.8 and 23.7°2θ, and a wide hump centered at 20.3°2θ). The Raman peaks produced by the plastic film can be easily subtracted from the Raman spectra of the samples. The post-XRD Raman measurement on the XRD sample sealed in this fashion showed that for all the hydrated magnesium sulfates that we studied, no detectable phase transformation occurred during the course of the XRD measurements (~7.5 min for a scan from 10° to 55°, 0.1° per step with 1 s dwell). Follow-up LRS measurements indicate that phase transformations in the sealed XRD sample holders eventually occur after 1–2 days. On the other hand, the most hydrated

Mg-sulfates (crystalline or amorphous) sealed in reaction vials do not show detectable phase changes even after 1–2 months of storage.

3.6. Raman measurements

A HoloLab5000 Raman spectrometer made by Kaiser Optical Systems Inc., (KOSI) was used in this study. This system uses the 532 nm line of a frequency-doubled Nd:YAG laser for excitation and has Stokes–Raman shifted spectral coverage of 50–4300 cm^{-1}. The spectral resolution is about 4–5 cm^{-1}. The wavelength of the CCD camera was calibrated using a standard neon emission lamp. The intensity throughput of the system was standardized against a secondary standard tungsten lamp using software provided by KOSI. The 0 cm^{-1} Raman shift of the excitation laser was set using the 801.3 cm^{-1} Stokes–Raman band of a cyclohexane standard, and was checked daily by measuring the Raman line 520.7 cm^{-1} of a wafer of single crystal Si. Deviations of the Si Raman line greater than ± 0.2 cm^{-1} were corrected by either shifting the Raman shift axis of the sample spectra or by resetting the 0 cm^{-1} of the laser line to the correct position using the KOSI software. With this calibration procedure, errors in accuracy and precision of Raman peak position measurements were kept to less than ± 0.2 cm^{-1}. An Olympus BX60 microscope fitted with a CCD image camera was coupled with the Raman spectrograph through two optical fibers; a single-mode optical fiber to transfer the excitation laser, and a 100 μm diameter optical fiber to transfer the collected Raman photons. A 20× microscopic objective (NA = 0.4) was used to focus the laser beam (6 μm in diameter) onto the sample and to collect the Raman photons produced by the sample. We generally employed a 15-mW laser light at the sample. The microscope was equipped with a software controlled, digital XYZ scanning stage, which had 0.1 μm as the smallest moving step, with >10 cm total moving distances in both X and Y directions perpendicular to the direction of the incident laser beam.

Using this Raman microprobe system, the Raman spectra of powdered samples (randomly oriented fine grains) in sealed reaction vials can be examined through the glass wall with 10× or 20× objectives. This sampling system permitted us to check routinely the progress of hydration/dehydration of the Mg-sulfates over various humidity-buffer solutions without altering the sample hydration state during the Raman measurements. Raman spectra of unstable hydrates of Mg-sulfates could also be readily obtained on the sample powder in XRD sample holders sealed with Saran Wrap® film or in the wells of microscope slides covered with a #1 or #11/2 cover slips. Unstable hydrates of Mg-sulfates remained unchanged in these sample containers for periods of hours or a day, whereas the Raman spectra of each sample could be recorded within minutes. In addition, using the 6 μm diameter laser beam focused with the 20× objective and a linear scan procedure, we could examine the heterogeneity in hydration states of a sample batch. This Raman point counting procedure, obtaining 50–100 Raman spectra at points of equal interval and requiring 10–20 min to complete, was conducted on the equilibrated Mg-sulfate samples and on the sealed XRD samples before and after the XRD measurements.

4. Results and discussion

Every S-bearing species has a characteristic Raman spectrum, because sulfur can form highly covalent chemical bonds both with itself and with other elements. Fig. 2 shows the typical Raman spectra of a set of S-bearing species that may exist in the sulfur cycle of a planet, including gas, liquid, elemental sulfur, sulfide, and sulfate. The Raman spectra for aqueous sulfates are quite dependent upon concentration, temperature, and pH. The middle three spectra in Fig. 2 can distinguish among various oxyanions of sulfur such as $[SO_3]$, $[HSO_4]^-$, $[SO_4]^{2-}$, H_3SO_5 and H_2SO_4 (Walrafen and Young, 1960; Young and Walrafen, 1961; Walrafen et al., 2002).

4.1. Raman spectra of 10 hydrated and anhydrous Mg-sulfates

We have recorded the Raman spectra from one anhydrous and nine hydrated Mg-sulfates prepared in this study. Fig. 3 shows these Raman spectra in the 400–1300 cm^{-1} spectral range dominated by the fundamental

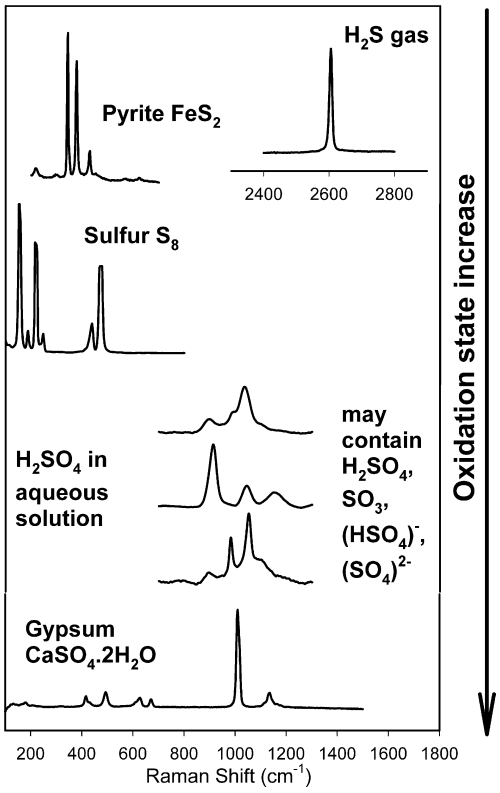

Fig. 2. Typical Raman spectra of S-bearing species that may exist in a planetary sulfur cycle.

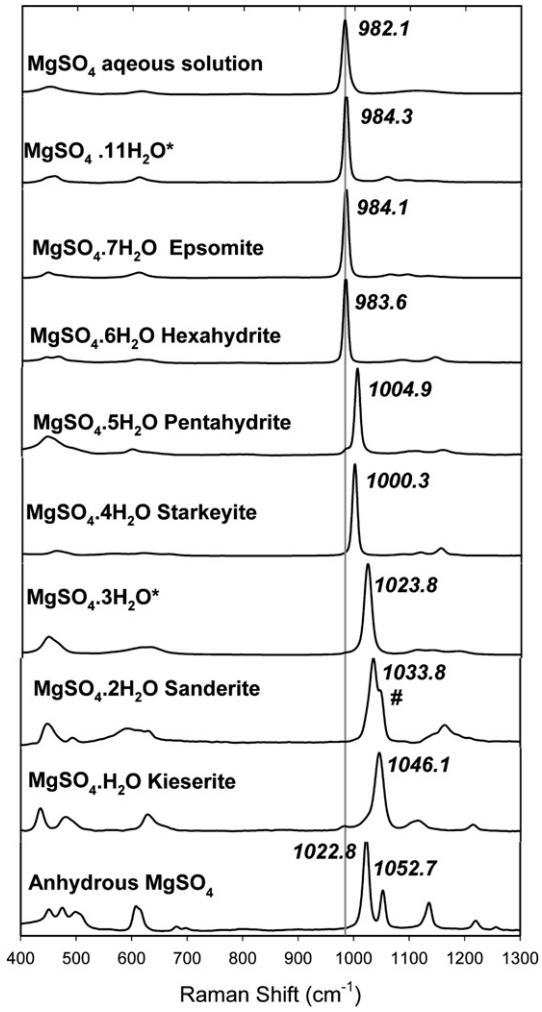

Fig. 3. Raman spectra of 10 hydrated and an anhydrous Mg-sulfates in the spectral region of SO_4 fundamental vibrational modes. *, Tentative spectral assignment; #, peak of kieserite as impurity.

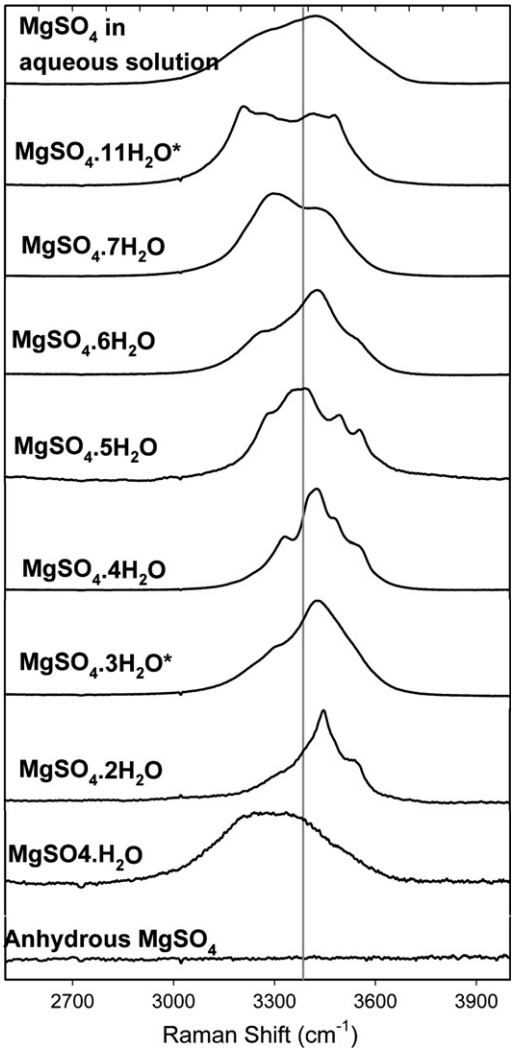

Fig. 4. Raman spectra of 10 hydrated and anhydrous Mg-sulfates in the spectral region of water OH stretching vibrational modes. *, Tentative spectral assignment.

vibrational modes of the SO_4 tetrahedra Fig. 4 shows the 2500–4000 cm^{-1} spectral range where the Raman peaks of structural water dominate. Table 3 lists the positions of the major Raman peaks of these Mg-sulfates.

Except for the $MgSO_4$ aqueous solution, $MgSO_4{\cdot}11H_2O$, and $MgSO_4{\cdot}3H_2O$, the Raman spectra assignments of the other seven Mg-sulfates in Figs. 3 and 4 have been confirmed by XRD measurements on the same samples using published values for the XRD powder diffraction patterns. The spectrum of $MgSO_4$ aqueous solution is obtained directly from a saturated solution within a liquid cell and the spectrum matches the data for neutral pH aqueous solutions of SO_4^{-2} obtained by Nakamoto (1997). We found no published X-ray diffraction pattern for $MgSO_4{\cdot}12H_2O$ that can be used to verify the Raman identification. Our assignment is based on the fact that (1) our sample was prepared according to the conditions shown in the phase diagram of Hogenboom et al. (1995) (i.e., the hydration of $MgSO_4 \cdot 7H_2O$ in equilibrium with ice at −5 °C); (2) the product shows a mass increase from the original mass of $MgSO_4{\cdot}7H_2O$ that is consistant with an increased degree of hydration; and (3) the LRS measurements on microscopically small crystals of several batches suggest a mixture of $MgSO_4{\cdot}7H_2O$ and a new phase. The spectrum of this new phase is tentatively assigned to $MgSO_4{\cdot}11H_2O$ (Figs. 3 and 4).

The Raman spectrum with a Raman peak at 1023.8 cm^{-1} is also tentatively assigned to $MgSO_4{\cdot}3H_2O$. The sample from which this spectrum was obtained was only produced once from hexahydrite powder baked in an oven at 60 °C in ambient-laboratory relative humidity. Raman point-counting measurements suggest that this sample is a mixture. Among numerous Raman spectra from this sample, we see Raman peaks of hexahydrite with a minor amount of kieserite, starkeyite, and sanderite, plus the Raman spectrum of a new phase with a unique Raman spectrum showing a v_1 peak at 1023.8 cm^{-1} and a distinct spectral pattern. Compared with the Raman v_1 peak positions of other hydrated Mg-sulfates whose identities were

Table 3
Raman peak positions of 10 hydrous and anhydrous Mg-sulfates

Hydrous and anhydrous Mg-sulfates	H_2O vib. modes		SO_4 vib. modes				Other peaks
	Stretching mode	Bending mode	v_1 mode	v_2 mode	v_3 mode	v_4 mode	
$MgSO_4$ in aqueous solution	3423 3292	1644	982.1	451	1113	617	366
$MgSO_4{\cdot}11H_2O$	3211 3263 3413 3479	1670 1679 (1673)	984.3	460 (446)	1059 1095 1133	611	371 251 205
Epsomite $MgSO_4{\cdot}7H_2O$	3303 3425 (3217)	1672	984.1	447 (459) (470)	1095 1134 1061	612	369 245 154
Hexahydrite $MgSO_4{\cdot}6H_2O$	3428 3258	1655	983.6	466 445	1146 1085 (1088) (1079)	610 (626)	364 245 223
Pentahydrite $MgSO_4{\cdot}5H_2O$	3391 3343 3553 3494 3289	1650	1004.9	447 371	1159 1106	602	241 206 165 119
Starkeyite $MgSO_4{\cdot}4H_2O$	3427 (3402) 3558 3481 3331	1603 1643 (1634) (1688)	1000.3	462 (480) 401	1156 1183 1116 (1119) (1114) 1086	616 (627) 664 565	313 240 150 109
$MgSO_4{\cdot}3H_2O$ (tentative)	3429 3308	1664	1023.8	449	1141 1189 1114	622	200 113
Sanderite $MgSO_4{\cdot}2H_2O$	3446 3539	1647	1033.8	447 492	1164	597 630	266
Kieserite $MgSO_4{\cdot}H_2O$	3297	1509	1046.1	436 481	1117 1215	629	272 218
Anhydrous β-$MgSO_4$			1022.8 1052.7	499 475 451	1136 1220 1256	608 681 697	205

Note: (1) peak position values were obtained from the spectra of fine ground powder samples with randomly oriented grains, data from several samples of each species were compared and compiled; (2) peak position values in ( ) were observed less commonly, possibly from crystal grains of different orientations; (3) the first peak position value in each vibrational mode of each species has the strongest intensity.

confirmed by powder XRD, e.g., 1033.8 cm^{-1} for $MgSO_4{\cdot}2H_2O$ (sanderite) and 1000.3 cm^{-1} for $MgSO_4{\cdot}4H_2O$ (starkeyite), a 1023.8 cm^{-1} v_1 peak position for this new phase suggests an Mg-sulfate with low degree of hydration. We assigned this spectrum to the trihydrate phase, because Raman spectra of all other hydrates of Mg-sulfate have been precisely assigned and verified by powder XRD data. We are currently attempting to reproduce a sufficient quantity of pure sample with this Raman spectral feature to verify its structure using XRD methods.

4.2. Systematic $[SO_4]^{2-}v_1$ peak position shift following the hydration degree changes

In the Raman spectra within the 400–1300 cm^{-1} spectral range (Fig. 3), the symmetric stretching vibration v_1 mode of SO_4 tetrahedra shows as the strongest Raman peak for each hydrated and anhydrous Mg-sulfate. This peak shifts upward, from 982.1 to 1052.7 cm^{-1} generally following the decrease of the degree of hydration. Unlike the peak position shift caused by the mass effect of cation substitutions in pyroxene (Wang et al., 2001), olivine (Kuebler et al., 2005), carbonates and sulfates (Herman et al., 1987; Kuebler et al., 2001), and Fe–Cr–Ti oxides (Wang et al., 2004a), these observed peak shifts arise solely from the variations of hydration state of the magnesium sulfates. Furthermore, the v_1 peak shift towards higher frequencies with decreasing water content, although it is not strictly monotonic. Minor deviations from a smooth trend exist for epsomite and hexahydrite, and for pentahydrite and starkeyite (Fig. 5). Also, the v_1 peak position of anhydrous Mg-sulfate falls away from the smooth trend. Nevertheless,

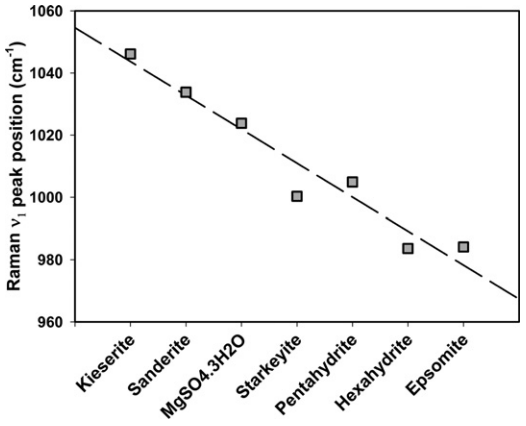

Fig. 5. Inverse correlation between the Raman v_1 peak position and the degree of hydration of Mg-sulfates.

a general inverse correlation exists between the position of the v_1 Raman peak position and the degree of hydration (Fig. 5). In addition to the strongest v_1 peak for each Mg-sulfate species, the other Raman peaks with weaker intensities also have patterns that are distinct among these species (Table 3). These peaks arise from other fundamental modes of SO_4 tetrahedra and the lattice modes involving the translational and librational modes of SO_4 and Mg ions and structural water.

Crystal structural variations are the general causes for the variations in Raman spectral patterns and the systematic shift of Raman peaks. In these Mg-sulfates, the v_1 Raman peak shift is a combinational effect caused by variations in linkages among SO_4 tetrahedra to $MgO_n(OH_2)_{6-n}$ octahedra, and in the amount of hydrogen bonding that affects the coordinating oxygen of SO_4 tetrahedra. Table 4 compares some structural details that may affect the observed vibrations of SO_4 tetrahedra. Complete crystal structure refinements, including neutron scattering for hydrogen atom positions, have been made for the following Mg-sulfates: anhydrous $MgSO_4$ (Rentzeperis and Soldatos, 1958), kieserite ($MgSO_4{\cdot}H_2O$, Aleksovska, 1998), starkeyite ($MgSO_4{\cdot}4H_2O$, Baur, 1964b), pentahydrite ($MgSO_4{\cdot}5H_2O$, Baur and Rolin, 1972), hexahydrite ($MgSO_4{\cdot}6H_2O$, Zalkin et al., 1964), and epsomite ($MgSO_4{\cdot}7H_2O$, Baur, 1964a). We have reconstructed the crystal structures of these phases (Fig. 6) using those data and PC software Diamond 2.1 (Crystal Impact, 1998–2002). Using this software program, we analyzed the effects of hydration state variations on bond lengths of SO_4 tetrahedra and on the linkages among the SO_4 tetrahedra and the $MgO_n(OH_2)_{6-n}$ octahedra. Tables 4 and 5 list some variations in the structures that may affect the Raman spectral features.

The SO_4 tetrahedra are connected to Mg cations in different ways within these Mg-sulfates, either by sharing a bridging oxygen (O_b in Table 4), or linked only by hydrogen bonding. For example in epsomite (Fig. 6a), the SO_4 tetrahedra are linked to the $Mg(OH_2)_6$ octahedra through hydrogen bonding with coordinated water molecules only. The lattice contains additional free water molecules that are not coordinated in any polyhedra. In starkeyite, each SO_4 tetrahedron is connected directly to Mg by sharing two bridging oxygen atoms (O_b), and this results in a four-member ring as the basic structural unit (Fig. 6b). The waters of hydration are only associated with the Mg. The four-member rings are connected weakly by the hydrogen bonding between the structural water and non-bridging oxygen (O_{nb}) on neighboring SO_4 tetrahedra. In kieserite (Fig. 6c), each SO_4 tetrahedron is tightly connected to four Mg octahedra by sharing coordinated oxygen (O_b). The effect of hydrogen bonding is less prominent.

In silicates, when the degree of polymerization of the SiO_4 tetrahedra increases (i.e., when the number of O_{nb} decreases), the v_1 symmetric stretching peak of SiO_4 tetrahedra shifts to higher wavenumbers: i.e. from ~860 to 950 cm^{-1} in olivine and garnet ($O_{nb} = 4$), to ~1000 cm^{-1} for pyroxene ($O_{nb} = 2$), to ~1000 to 1100 cm^{-1} in amphibole ($O_{nb} = 1.5$), and to ~1100 to 1150 cm^{-1} in mica ($O_{nb} = 1$). This trend was attributed to the linkage to a 2nd (or 3rd) Si tetrahedron that affects the symmetric stretching vibrational mode of SiO_4 as an ionic group (McMillan, 1984; Wang et al., 1994). Similar mechanisms may also be used to interpret the peak-position shift in

Table 4
A comparison of the structural details related to Raman peak positions of the SO_4 ionic group (from crystal refinement data in references a–f of Table 2)

Mg-sulfates with known structure	S–O_{nb} bonds in SO_4	S–O_b[b]–Mg linkage	No. of H-bonds that affect individual oxygen ions in SO_4			
	No. of O_{nb} in SO_4	No. of O_b in SO_4	Total No. of H-bonds affecting SO_4	O_{nb}[a]	O_b[b]	Average length (Å) of H-bonds
$MgSO_4$	0	4 (O_i & O_{ii})	0	0	0	
$MgSO_4{\cdot}H_2O$	0	4 (O_1 & O_2)	1		1 for O_2[c]	1.806
$MgSO_4{\cdot}4H_2O$	2 (O_{iii} & O_{iv})	2 (O_i & O_{ii})	8	3 for O_{iii}, 3 for O_{iv}.	1 for O_i, 1 for O_{ii}.	1.955
$MgSO_4{\cdot}5H_2O$	2 (O_3 & O_4)	2 (O_1 & O_2)	8	2 for O_3, 3 for O_4.	1 for O_1, 2 for O_2.	1.923
$MgSO_4{\cdot}6H_2O$	3 (O_1, O_3, O_4)	1 (O_2)	10	2 for O_1, 2 for O_3, 3 for O_4.	3 for O_2	2.061
$MgSO_4{\cdot}7H_2O$	4	0	10	2 for O_1, 2 for O_2, 3 for O_3, 3 for O_4.	0	1.834

[a] O_{nb}, oxygen ion in the SO_4 group that is not linked to any Mg cation.
[b] O_b, oxygen ion in the SO_4 group that is linked to an Mg cation.
[c] $O_{1,2,3,4}$ or $O_{i,ii,iii,iv}$, the symbols used in structural refinement results of that compound.

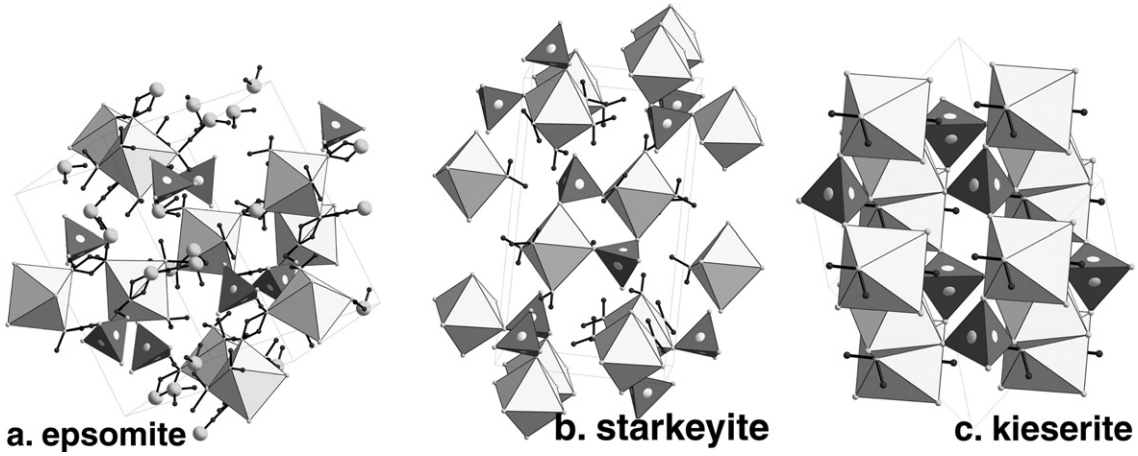

Fig. 6. Crystal Structures of three hydrated Mg-sulfates: (a) epsomite; note that SO_4 tetrahedra are only linked to $Mg(OH_2)_6$ through hydrogen bonding and note the existence of free H_2O molecules; (b) starkeyite; note the four-member ring made by two SO_4 tetrahedra and two $MgO_2(OH_2)_4$ octahedra; and (c) kieserite; note that each oxygen ion in the SO_4 group is connected directly to a Mg cation.

hydrated Mg-sulfates of this study: the lower the number of O_{nb} in the SO_4 tetrahedron, the higher the position of the v_1 peak (kieserite has $O_{nb} = 0$ and a Raman peak at 1046.1 cm^{-1}, Tables 3 and 4). We note that the analogy between connected SiO_4 tetrahedra in the silicates and the connected SO_4 tetrahedra and Mg-polyhedra in Mg-sulfates is not strictly equivalent because the strength of the bonding in S–O_b–Mg is much weaker than the covalent bonding in Si–O_b-Si. Owing to the lower electronegativity of Mg compared to Si, the extent of the peak shift is therefore much smaller in Mg-sulfates ($\sim$70 cm^{-1}) than in silicates ($\sim$300 cm^{-1}).

In addition to the effect of S–O_b–Mg bonds, we think the hydrogen bonding to coordinated oxygen in SO_4 tetrahedra plays a concomitant role in producing the systematic shift of v_1 Raman peak positions in these hydrated Mg-sulfates. The normal effect of hydrogen bonding to the oxygen of an M–O bond is to shift the vibrational peak of M–O bond to lower wavenumbers. Regarding this point, we note that the number of total H-bonds that affect the coordinated oxygen ions in SO_4 tetrahedra increases following the increase of the hydration degree from one in kieserite to ten in epsomite (Table 4). This increase is accompanied by a consistent tendency of the v_1 Raman peak position of SO_4 tetrahedra to shift downward, e.g., the structure of epsomite and hexahydrite have the highest number (10) of H-bonding that affect the coordinated oxygen in SO_4 tetrahedra per formula unit and the v_1 Raman peak positions (984.1 and 983.6 cm^{-1}) at the very low end of the full range (Tables 3 and 4).

4.3. Water-band shape variations and sub-peak position changes

The broad Raman band in the 2500–4000 cm^{-1} spectral region (Fig. 4) consists of the v_1 symmetric stretching, the weaker v_3 asymmetric stretching, and the 1st overtone of the v_2 bending mode of the water molecule. Among the 10 hydrated and anhydrous magnesium sulfates, we observe changes in the positions of the maximum and in the overall band shape following the change of hydration states. For each species except anhydrous $MgSO_4$ and kieserite, the broad water band is made of several sub-peaks, and the number of sub-peaks and their positions change following the number of structural water molecules in hydrated Mg-sulfates. Table 3 lists the positions of these sub-peaks.

In five known hydrated magnesium sulfate structures (Baur, 1964a,b; Zalkin et al., 1964; Baur and Rolin, 1972; Aleksovska, 1998), each of the structural waters occupies a distinct crystallographic site. For example, starkeyite has four distinct crystallographic sites for its four structural water molecules (O_{w1}, O_{w2}, O_{w3}, O_{w4} in Table 5, the notation follows that used in the original structural refinement), while pentahydrite has five, hexahydrite has six, epsomite has seven, and kieserite has only one. From the structural refinements using neutron diffraction data, it appears that the shape of each structural water molecule can be severely distorted from the shape of a free water molecule, apparently affected by the site symmetry. The two O–H bonds (O–H_1 and O–H_2 columns of Table 5) in one water molecule can have different bond lengths. For example, a water molecule with O_{7w} as the central oxygen in hexahydrite has two O–H bond lengths of $L_{O-H1} = 0.447$ Å and $L_{O-H2} = 1.093$Å. Although Table 5 lists only the changes in O–H bond length, similar changes in H–O–H bond angles are also present. The change in the molecular shape would in turn result in a set of shifted Raman peaks in the 2500–4000 cm^{-1} spectral region. When the molecular shape distortions are less severe, the individual molecule retains its basic symmetry but average bond lengths vary from one site to another (cf., starkeyite and pentahydrite in Table 5). In theses cases, the individual peaks from water molecules of distinct crystallographic sites would occur near each other and would sometimes overlap to become a broad spectral band with distinct sub-peak structure, e.g.,

Table 5
The length of OH bonds in five known hydrated Mg-sulfate structures (from crystal refinement data in references a–f of Table 2)

	Oxygen in structural water	OH bond length (Å)		All OH bonds in compound		
		$O–H_1$	$O–H_2$	Average OH bond length (Å)	Max. variation of OH bond length (Å)	Largest variation of OH bond length (%)
Kieserite	O_{3w}[b]	0.984	0.984	0.984	0.000	0
Starkeyite	O_{w1}	0.951	0.969	0.962	0.059	6
	O_{w2}	**0.931**[a]	0.968			
	O_{w3}	0.951	**0.99**			
	O_{w4}	0.958	0.98			
Pentahydrite	O_{W5}	0.97	0.975	0.972	0.014	1
	O_{W6}	0.971	**0.982**			
	O_{W7}	0.97	0.973			
	O_{W8}	**0.968**	0.969			
	O_{W9}	0.968	0.97			
Hexahydrite	O_{5w}	0.818	0.835	0.832	0.646	78
	O_{6w}	0.752	0.974			
	O_{7w}	**0.447**	**1.093**			
	O_{8w}	0.834	1.025			
	O_{9w}	0.688	0.844			
	O_{10w}	0.775	0.9			
Epsomite	O_{w1}	0.957	0.989	0.979	0.35	36
	O_{w2}	0.87	1.035			
	O_{w3}	0.977	**1.216**			
	O_{w4}	**0.866**	1.101			
	O_{w5}	0.869	0.897			
	O_{w6}	0.944	0.988			
	O_{w7}	0.996	1.006			

[a] Bold numbers indicate the longest or shortest O–H bond in the compound.
[b] The symbols used in the structural refinement work of that compound.

the Raman band of structural water in amphiboles (Wang et al., 1988). This type of band complexity is seen in the spectra of some hydrated Mg-sulfates, e.g., starkeyite and pentahydrite (Fig. 4).

In the case of hexahydrite (and epsomite), a higher number of structural water molecules is contained in a much less compact crystal structure (the density of hexahydrite is only 12% that of starkeyite). Here, some structural water molecules take a very irregular shape, i.e., the two O–H bonds of a water molecule can have very different bond lengths with significant molecular asymmetry (e.g., water with O_{7w} in hexahydrite). When using the maximum O–H bond length variation (in % over the average O–H bond length in a structure) to evaluate the degree of asymmetry of the water molecules in a compound (Table 5), the values for hexahydrite and epsomite are 78% and 36%, respectively, in comparison with 1% for pentahydrite and 6% for starkeyite. We consider that the irregular shapes of the water molecules in hexahydrite and epsomite structures could be the cause for the less obvious sub-peak structure of their water bands (Fig. 4).

We obtained a Raman band in the OH stretching vibrational region (2500–4000 cm^{-1}) with very distinct sub-peak structure from an Mg-sulfate phase that was equilibrated from epsomite over the 100% relative humidity buffer at −5 °C. Several batches of samples (in powder and crystal forms) under similar conditions were made and examined in order to check the reproducibility of this spectral feature. This particular water band is compared with the water band of crystalline epsomite and starkeyite in Fig. 7, with the latter two taken from the crystals grown from solutions and measured at two distinct crystal orientations relative to a partially polarized laser beam. This comparison confirms that this particular water band is not produced from the crystal orientation effect on the water band of epsomite, but rather arises from a new hydrated magnesium sulfate phase. This phase is assigned to $MgSO_4{\cdot}11H_2O$, the only known Mg sulfate having higher hydration state than epsomite (or $MgSO_4{\cdot}11H_2O$ based on Peterson and Wang, 2006). This assignment is tentative, however, because the structural refinement for $MgSO_4{\cdot}11H_2O$ becomes available only recently (Peterson and Wang, 2006). The ν_1 peak position (984.3 cm^{-1}) of this new phase is almost the same as that of epsomite (984.1 cm^{-1}), although having minor peaks at slightly different positions (Table 3). Similarly, a very small peak-position difference is noticed for the ν_1 peaks of hexahydrite and epsomite (983.6 and 984.1 cm^{-1}), with epsomite having an additional structural water molecule that is not connected to any SO_4 and $Mg(OH_2)_6$ polyhedra. We consider, based on similar reasoning, that the very similar ν_1 peak positions of $MgSO_4{\cdot}11H_2O$ and epsomite may mean that the additional

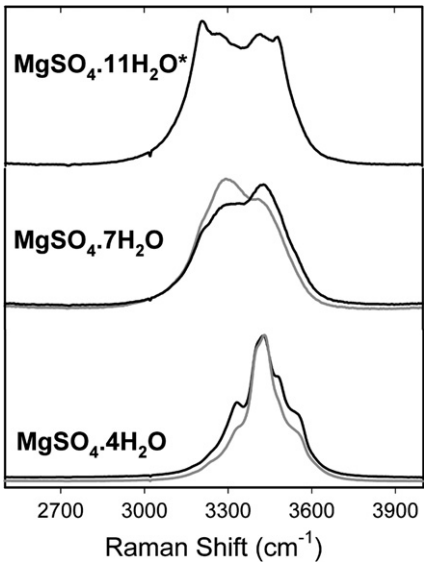

Fig. 7. The Raman water band from a new phase (tentatively assigned to $MgSO_4{\cdot}11H_2O$) compared with those of epsomite and starkeyite at two distinct crystal orientations. *, Tentative spectral assignment.

five structural water molecules in $MgSO_4{\cdot}11H_2O$ could occur in the spaces among the polyhedra, without directly bonding to either SO_4 or $Mg(OH_2)_6$ polyhedra.

4.4. Stability fields and pathways of phase transitions using anhydrous Mg-sulfate as starting material

Using the characteristic Raman peaks of the Mg-sulfates, we can identify the corresponding hydration states of Mg-sulfates directly from the raw spectrum of a mixture. The Raman point scan with a microbeam laser stimulation will allow determination of the spatial distribution of the phases in fluid-solid interactions, and of the relative proportions of co-existing species. This information permits us to study the stability field of these species under different temperatures and relative humidities, and to simulate (or to extrapolate) the reactions that might occur during a martian diurnal cycle. Results of this study and of previous studies (Chou and Seal, 2003; Vaniman et al., 2004, 2005; Chipera et al., 2005; Chou et al., 2005) indicate that phase transitions tend to occur rapidly at the initial stage, but are typically sluggish in the attainment of final equilibrium, thus it is not easy to achieve equilibrium during the diurnal cycle on Mars. It is thus very important to study not only the apparent final reaction products but also the pathways of the phase transitions, i.e., the dehydration and re-hydration processes of crystalline and non-crystalline species. Knowledge of reaction pathways and products bear importantly on the interpretations of spectral observations by the Mars Express OMEGA instrument, as well as on data from future landed missions.

The Raman ν_1 peaks of SO_4 tetrahedra from ~982.1 to ~1052.7 cm^{-1} are especially suitable to identify the different hydrated Mg-sulfates in mixtures, because the narrow peak width allowing visual resolution of individual peaks

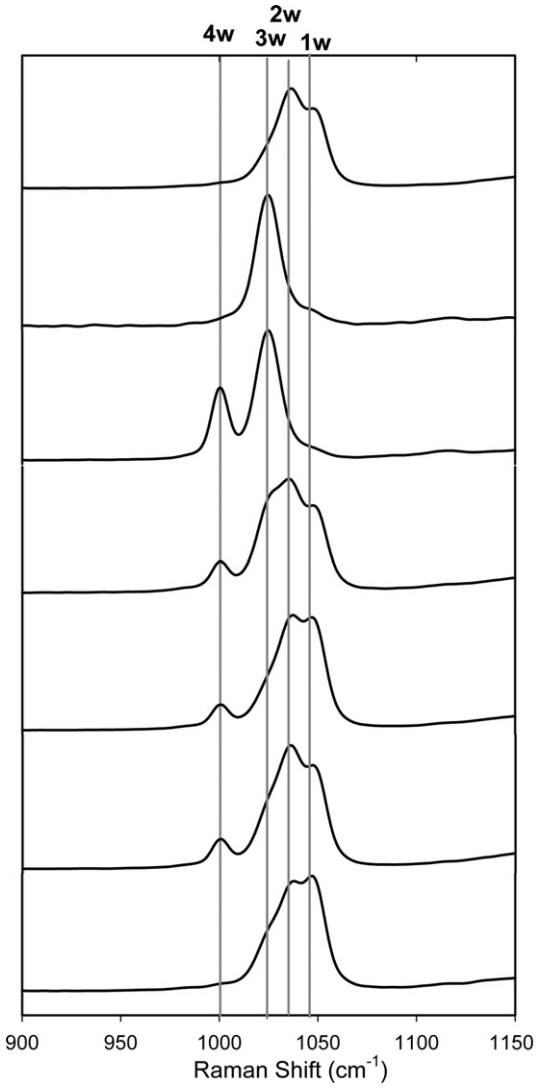

Fig. 8. Raman spectra from different spots on a Mg-sulfate sample prepared at 60 °C and ~7% RH, which suggest the coexistence of starkeyite, $MgSO_4{\cdot}3H_2O$, sanderite, and kieserite.

from the spectrum of mixture and the systematic peak position shift identify directly the degree of hydration. Fig. 8 shows a set of Raman spectra in the 900–1150 cm^{-1} range, taken at various locations in a sample prepared at 60 °C and ~7% RH using hexahydrite as the starting material. These spectra demonstrate the coexistence of kieserite, $MgSO_4{\cdot}3H_2O$, sanderite, and starkeyite in the resulting mixture, with varying ratios of peak intensity. The phase heterogeneity of this sample was studied using the 20× objective of the Raman microprobe (6 μm diameter condensed laser beam at sample focus) in a 200 points linear scan across the surface of the sample. Raman spectra of multiple hydrate phases like those shown in Fig. 8 were observed from every sampling spot. This means that the laser beam encountered several different hydration states within each sampled volume, which may result either from extremely tiny grains packed closely together (~6μm), or the same grain containing zones of different hydrations

within larger crystal. Among the 200 Raman spectra recorded, the number of times that the different phases appear in the Raman spectra are as follows: kieserite—177; sanderite—43; $MgSO_4{\cdot}3H_2O$—195; starkeyite—199; hexahydrite—54. In the Raman point-counting procedure, we do not use the relative peak intensities of every species to calculate its relative proportion in the mixture because the peak intensities are dependent on Raman cross-sections (currently unknown for hydrated Mg-sulfates). Instead, we use the frequency of appearance of characteristic peaks of each species in the set of 50–200 spectra to estimate their relative proportions (Haskin et al., 1997).

We have begun a study of stability fields of various hydrated Mg-sulfates where we use the relative humidity buffer solutions at fixed temperature to drive the de-hydration or re-hydration process. The anhydrous $MgSO_4$ at 50 °C and seven relative humidities (11.1%, 30.5%, 50.9%, 64.5%, 74.4%, 84.8%, and 100% RH) were investigated first. Raman spectroscopy and mass-change measurements were used to monitor the progress of hydration by frequently measuring the intermediate products. XRD measurements were made on some final products to verify specific Raman identifications.

At 50 °C in these experiments, the initial hydration species of anhydrous Mg-sulfate were observed almost immediately (within 1 day), but the rates of hydration, the amounts and types of intermediate phases, and the final equilibrium phase(s) were quite dependent upon the RH of the environment (Table 6). Fig. 9 presents some typical Raman spectra obtained from this set of experiments.

No trace hydration of anhydrous $MgSO_4$ was observed through a 1-month reaction at 11.1% RH and 50 °C. Nevertheless, a trace of sanderite ($MgSO_4{\cdot}2H_2O$) was observed after 18 h at 30.5% RH, which showed a progressively strengthened water band with maximum ~3446 cm^{-1} and the appearance of a shoulder ~1033.8 cm^{-1} between the two Raman peaks of anhydrous $MgSO_4$ (1052.7 and 1023.8 cm^{-1}). From day 4 through day 40, this spectral pattern did not change at all, suggesting the equilibrium was reached.

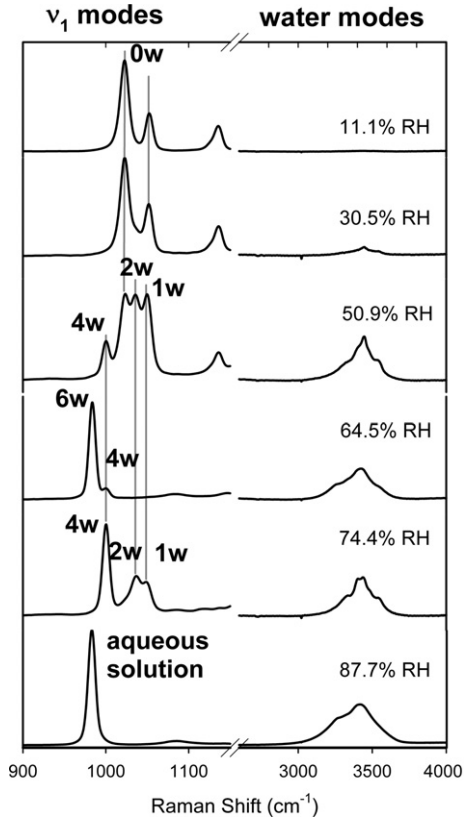

Fig. 9. Raman spectra of hydration products (at different stages of process) from the experiments of anhydrous β-$MgSO_4$ at 50 °C and various humidity buffers.

Table 6
Hydrated Mg-sulfate phases observed during the hydration progress of anhydrous $MgSO_4$ at 50 °C under different relative humidity at 1 atm

Humidity buffers	LiCl[a]	$MgCl_2$	NaBr	KI	NaCl	KNO_3	H_2O
RH (%)	11.1	30.5	50.9	64.5	74.4	84.8	100
18 h[c]		0w, 2w		4w, 0w			4w, 6w[b]
Day1	**0w**[d]		0w, 2w, 4w		0w, 2w, 4w	4w, 0w	
Day2	0w		0w, 2w, 4w		0w, 2w, 4w	4w	
Day4		**0w**, **2w**		4w, 6w			6w, solution
Day7	0w		1w, 2w, 3w, & weak 4w		1w, 2w, 4w, & weak 3w	**6w**, **solution**	
Day8			1w, 2w, 3w, & weak 4w		4w, 1w, 2w, & weak 3w		
Day13	0w		**4w**, **1w**, **2w**		**6w**	6w, solution	**Solution**
Day14		0w, 2w		6w, 4w			
Day15	0w		4w, 1w, 2w		6w	6w, solution	
Day21		0w, 2w		**6w**			
Day22		0w, 2w		6w			
Day27	0w	0w, 2w		6w			
Day29		0w, 2w		6w			

[a] Salts in saturated aqueous solutions for maintaining constant relative humidity.
[b] Identifications made by Raman spectroscopy: 0w, anhydrous $MgSO_4$; 1w, kieserite; 2w, sanderite; 3w, $MgSO_4{\cdot}3H_2O$; 4w, starkeyite; 6w, hexahydrite; solution, Mg^{2+} and SO_4^{2-} in aqueous solution.
[c] Duration of anhydrous $MgSO_4$ kept in the humidity buffers.
[d] Bolded words are the Mg-sulfate phases in the final steady state at 50 °C and the listed RH.

At 50.9% RH and 50 °C, minor amounts of sanderite and starkeyite ($MgSO_4{\cdot}4H_2O$) appeared simultaneously within 1 day. Anhydrous $MgSO_4$ disappeared totally by day 7, accompanied by the appearance of $MgSO_4{\cdot}3H_2O$ and kieserite ($MgSO_4{\cdot}H_2O$). The coexistence of kieserite, sanderite, $MgSO_4{\cdot}3H_2O$, and starkeyite only lasted for a few days, then $MgSO_4{\cdot}3H_2O$ disappeared first, followed by gradually reduced peak intensities of kieserite and sanderite. Starkeyite became the dominant phase after day 15, accompanied by minor amounts of kieserite and sanderite as final products.

For the experiments done at 64.5% RH and 74.4% RH at 50 °C, starkeyite ($MgSO_4{\cdot}4H_2O$) appeared within 1 day. Both systems reached apparent equilibrium by total conversion to hexahydrite, but the system at 74.4% RH reached apparent equilibrium earlier (after 13 days) than that at 64.5% RH (after 21days). Nevertheless, the system at 74.4% RH went through an intermediate step with coexisting kieserite, sanderite, $MgSO_4{\cdot}3H_2O$, and starkeyite; whereas the system at 64.5% RH had a mixture of starkeyite and hexahydrite at an intermediate step.

Even for the systems at 84.8% and 100% RH and 50 °C, starkeyite is found among the early hydration products. The system at 84.8%RH converted completely to starkeyite by day 2. Hexahydrite appears also at an early stage of hydration (in 18 h for 100% RH and at day 7 for 84.8% RH). Deliquescence is the equilibrium product for the samples at both RHs, and the system at 100% RH reached this stage earlier than the one at 84.8% RH.

In these preliminary experiments, the equilibrated phases at relative humidity $\geqslant$65% are consistent with the phase diagram obtained by Chou et al. (2005). At lower humidity, starkeyite, sanderite, kieserite, and anhydrous $MgSO_4$ remain in the final mixtures. We note that the phase transitions among most of the hydrated magnesium sulfates involve significant crystal structure rearrangement (Table 2). This structural rearrangement requires additional energy to overcome activation energy barriers. In contrast, the phase transitions between hexahydrite and epsomite (and maybe $MgSO_4{\cdot}11H_2O$) involve mainly the addition/or removal of the interstitial water molecules that were not coordinated with any polyhedra. Therefore, it may be structurally easier to reach final equilibria at high RH than at mid-to-low RH. The observed final products at mid-to-low RH in the experiments described above may reflect the metastability of certain hydrated species, sluggish kinetics for some, and path dependence, as observed by Chipera et al. (2005). Owing to the structural rearrangements involved in the reactions, the initial structure is an important factor for the pathway of phase transitions. We are therefore continuing the experiments using four of the most common (on Earth and most-likely on Mars) Mg-sulfates as starting materials, i.e., kieserite, starkeyite, epsomite, and amorphous Mg-sulfates with more humidity buffers (10 in total), and multiple temperatures.

4.5. Amorphization from rapid dehydration

Vaniman et al. (2004, 2005) suggested that during the diurnal cycle on Mars, when temperature changes over 100 °C and relative humidity swings from almost 0% to 100%, the rapid dehydration of hydrous Mg-sulfates (epsomite and hexahydrite) would produce an amorphous Mg-sulfate, evidenced by the loss of all diffraction lines in an X-ray diffraction pattern. Because the re-hydration of this XRD-amorphous phase is extremely sluggish under the current martian surface conditions, Vaniman et al. (2004, 2005) suggested that non-crystalline $MgSO_4$, not kieserite, would be the most commonly observed phase at equatorial regions on the martian surface.

We conducted a rapid dehydration experiment by placing finely powdered (<75 μm) crystalline epsomite ($MgSO_4{\cdot}7H_2O$; XRD pattern shown in Fig. 10a) into a desiccator under vacuum at room temperature (21 ± 1 °C). Active vacuum was held at ~0.5 torr (~67 Pa) for 15 days. The mass-change measurement of the end-product indicates that each epsomite molecule lost ~5.1 water molecules on average. Consistent with the result of Vaniman et al. (2004), this product is XRD-amorphous (Fig. 10b). A broad featureless hump centered ~29° 2θ remains in the X-ray diffraction pattern, which indicates the transformation of the original orthorhombic structure (epsomite) to a non-crystalline structure.

Although, the end-product of this rapid dehydration has a featureless XRD pattern, its Raman spectrum (Fig. 10c) still contains many characteristic spectral features that re-

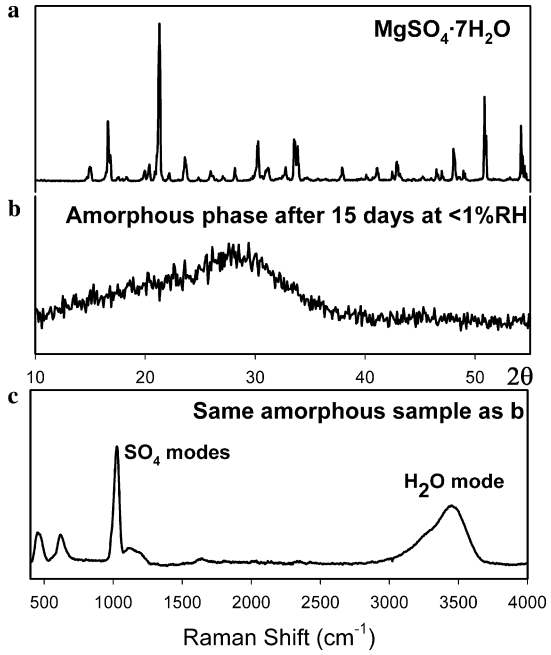

Fig. 10. Amorphous Mg-sulfate formed from rapid dehydration of epsomite: (a) XRD pattern of epsomite as starting material, (b) XRD pattern of dehydration product after putting epsomite powder in vacuum for 15 days at room temperature, and (c) Raman spectrum of the same dehydration product.

veal its hydration state and low-crystallinity features. In particular, the broadening of the Raman bands and resulting loss of fine spectral details (which are normally associated with the spectrum of a crystalline material) clearly indicates an amorphous material was formed by rapid dehydration.

Unlike XRD, the translational symmetry in a structure is not a necessary condition to produce Raman and infrared spectra. Gases, liquids, and glasses all have characteristic vibrational spectral peaks, because they are produced by the vibrations of chemical bonds. Nevertheless, the structural distortion or amorphization in solids such as glasses, polymers, and disordered crystalline lattices, arising during rapid changes in chemical composition or shocks due to sudden changes in pressure and/or temperature, will change the peak parameters in their vibrational spectra. Thus the crystalline and amorphous forms of a chemically identical species can generally be distinguished. Typically, Raman peak width is the first spectral parameter to be affected by the loss of crystallinity. The loss of translational symmetry would affect the environmental symmetry of a site where an anionic group resides (e.g., SO_4 group in sulfate). Slight structural distortion (bond lengths and bond angles) of the SO_4 group could be introduced, which would translate into a v_1 peak position slightly different from that of an SO_4 group in a regular crystalline structure. The contributions from many irregularly distorted SO_4 groups would produce a broad Raman peak, i.e., an envelope of many peaks with slightly different peak positions. The higher the degree of amorphization, the broader the Raman peak width.

The Raman spectrum of the end-product of rapid dehydration from epsomite shows a prominent water band in the 2500–4000 cm^{-1} spectral region (Fig. 11a), with a maximum centered at 3460 cm^{-1} and a shoulder at ~3290 cm^{-1}, which clearly indicates a hydrated species. In the fundamental vibration region (950–1150 cm^{-1}), this phase shows a v_1 peak with much wider peak width than any crystalline hydrated or anhydrous Mg-sulfates, including $MgSO_4$ in an aqueous solution (Fig. 11a). This broadened peak width is indicative for a heavily disordered non-crystalline structure. The maximum of the broad peak for a 15-day dehydration product at room temperature is centered at ~1030 cm^{-1}. This peak position (Fig. 11a) lies between the v_1 peaks of starkeyite ($MgSO_4{\cdot}4H_2O$, 1000.3 cm^{-1}) and kieserite ($MgSO_4{\cdot}H_2O$, 1046.1 cm^{-1}), and suggests a hydration state within the range of $MgSO_4{\cdot}3H_2O$ (1023.8 cm^{-1}) and $MgSO_4{\cdot}2H_2O$ (1033.8 cm^{-1}). The assignment of hydration degree based on the Raman peak position is consistent for the most part with the result of mass-change measurements, i.e., a product with an average hydration degree of $MgSO_4{\cdot}1.9H_2O$. The loss in crystallinity of epsomite by evacuation at ambient temperature can occur very quickly. Fig. 11b shows that the loss of crystallinity began within the first 30 min, and a shift upward of the v_1 peak position of SO_4 was observed during the progress of dehydration, evidenced by the decreasing intensity

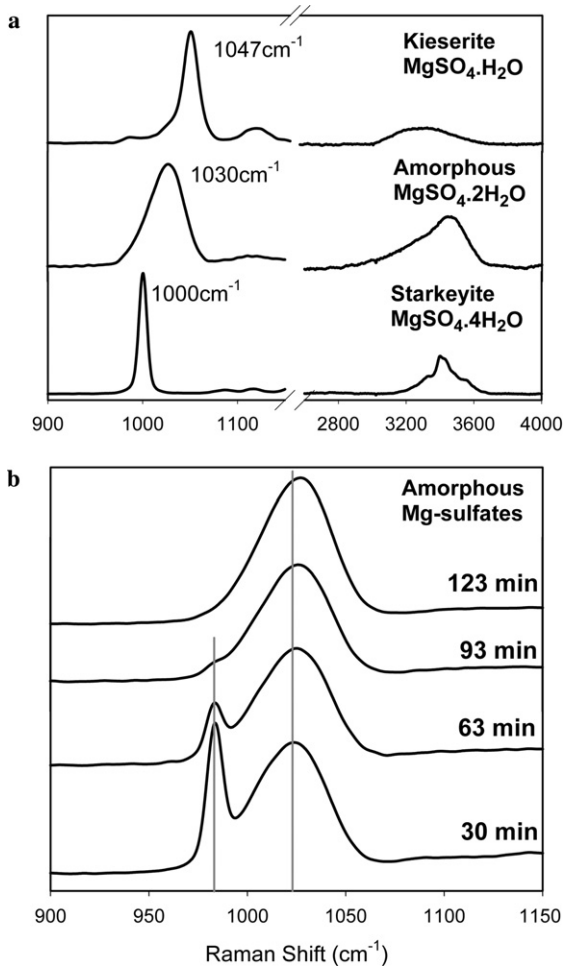

Fig. 11. (a) Comparison of the Raman spectra of an amorphous Mg-sulfate with starkeyite and kieserite; (b) Comparison of the Raman v_1 peak positions of amorphous Mg-sulfates formed after rapid dehydration of epsomite for various durations.

of the epsomite v_1 peak at ~984.1 cm^{-1}. These observations suggest that this peak-position variation of non-crystalline Mg-sulfates can also be used to evaluate their degree of hydration.

The conversion of hexahydrite to the amorphous dihydrate was also observed after a similar dehydration process at room temperature, where a loss of four molecules of water per molecule of sulfate was observed. Conversely, no weight loss was observed nor did any changes occur in the Raman spectra of either crystalline kieserite and starkeyite samples subjected to the same vacuum dehydration at room temperature. In the crystal structures of kieserite and starkeyite, the water molecules are more tightly coordinated with Mg cations, and the Mg polyhedra are tightly connected with SO_4 tetrahedra by sharing the bridging oxygen (O_b), which make their structures very stable towards vacuum dehydration. In comparison, the crystal structures of hexahydrite and epsomite are more loosely packed, evidenced by the larger volume per formula unit (2.5–2.8 times of kieserite when

normalized for $Z = 4$). The water molecules in epsomite and hexahydrite are associated with the Mg polyhedra and are only linked to SO_4 tetrahedra by hydrogen bonding, with the 7th water molecule not coordinated to any of the polyhedra in epsomite. The rapid loss of water molecules from these two higher hydrates would thus cause the crystal framework to collapse producing the observed amorphous phases.

5. Conclusions

Magnesium sulfates are found on Mars by orbital remote sensing and landed surface exploration missions. Reports of the data from these missions, especially those from the Mars Exploration Rovers, the GRS on Mars Odyssey, and OMEGA on Mars Express, suggest that magnesium sulfates with degrees of hydration higher than kieserite may exist at the martian surface in equatorial regions.

In this study, we demonstrated that crystalline Mg-sulfates with nine different hydration states can be readily distinguished using the systematic peak-position shift of their Raman v_1 mode and the specific sub-peak structures in their Raman water bands. In addition, $[SO_4]^{2-}$, $[HSO_4]^-$ and SO_3 in aqueous solutions, SO_2 and H_2S as gases, as well as elemental sulfur, sulfides, and sulfates that may participate in the martian sulfur cycle, all have diagnostic Raman spectra and thus can be characterized during hydration, dehydration, oxidation, and reduction processes, in mixtures, and at intermediate steps during phase transitions. Amorphous Mg-sulfates produced in rapid dehydration of epsomite and hexahydrite yield characteristic Raman spectra that reveal their hydration states and disordered structures.

The systematic Raman spectroscopic study of hydrated Mg-sulfates presented in this paper provides the essential basis for using planetary Raman spectroscopy to characterize, *in situ*, the hydration state and variation in crystallinity, and to monitor the phase transitions likely to occur (now or in the past) when the martian surface conditions change, as well as to understand the pathways of phase transitions as a function of initial structures, and of temperature and relative humidity excursions.

Studies of the phase stability fields and the phase transition pathways of Mg-sulfates (crystalline or non-crystalline), and the *in situ* characterization of their hydration states are extremely important in future planetary surface exploration. The combination of these two types of information will enable assessments of the current geochemical processes active at the martian surface as well as an improved understanding of martian hydrologic history, the cycles of water and sulfur, and the potential for past or present habitability.

Acknowledgments

Ben Greenhagen and Peter Scully helped with the sample preparation and characterization in the early parts of this study. Bill Feldman provided the assessment of the GRS data in the vicinity of Gusev Crater. Dave Vaniman gave constructive advice on sample preparation. Bjorn Mysen, Robert Seal, Harvey Belkin, Robert Downs, and an anonymous reviewer provided constructive reviews. We are thankful for the assistance of each of these individuals. This work is supported by NASA Grants NAG5-12684 (Mars Fundamental Research) and NAG5-10703 (Planetary Instrument Definition and Development). *The use of trade, product, industry, or firm name in this report is for descriptive purpose only and does not constitute endorsement by us or by the U.S. Government.*

Associate editor: Bjorn Mysen

References

Aleksovska, S., 1998. Calculation of structural parameters in isostructural series: the kieserite group. *Acta Cryst.* **B54**, 564–567.

Arvidson, R.E., Poulet, F., Bibring, J.-P., Wolff, M., Gendrin, A., Morris, R.C., Freeman, J.J., Langevin, Y., Mangold, N., Bellucci, G., 2005. Spectral reflectance and morphologic correlations in eastern Terra Meridiani, Mars. *Science* **V307**, 591–1593 (10.1126/science. 1109509).

Baur, W.H., 1964a. On the crystal chemistry of salt hydrates. IV. The refinement of the crystal structure of $MgSO_4{\cdot}7H_2O$ (epsomite). *Acta Cryst.* **17**, 1361–1369.

Baur, W.H., 1964b. On the crystal chemistry of salt hydrates. II. A neutron diffraction study of $MgSO_4{\cdot}4H_2O$. *Acta Cryst.* **17**, 863–869.

Baur, W.H., Rolin, J.L., 1972. Salt hydrates. IX. The comparison of the crystal structure of magnesium sulfate pentahydrate with copper sulfate pentahydrate and magnesium chromate pentahydrate. *Acta Cryst.* **B28**, 1448–1455.

Bibring, J.-P., Langevin, Y., Gendrin, A., Gondet, B., Poulet, F., Berthe, M., Soufflot, A., Arvidson, R.E., Mangold, N., Mustard, J.F., Drossart, P., 2005. Mars surface diversity as observed by the OMEGA/Mars Express investigation. *Science* **V307**, 1576–1581 (10.1126/science. 1108806).

Boynton, W.V., Feldman, W.C., Squyres, S.W., Prettyman, T.H., Brückner, J., Evans, L.G., Reedy, R.C., Starr, R., Arnold, J.R., Drake, D.M., Englert, P.A.J., Metzger, A.E., Mitrofanov, I., Trombka, J.I., d'Uston, C., Wänke, H., Gasnault, O., Hamara, D.K., Janes, R.L.M.D.M., Maurice, S., Mikheeva, L., Taylor, G.J., Tokar, R., Shinohara, C., 2002. Distribution of hydrogen in the near surface of Mars: evidence for subsurfac ice deposits. *Science* **297**, 81–85.

Carr, M., 1996. *Water on Mars*. Oxford University Press, Oxford.

Carr, M., Head, J., 2003. Oceans on Mars: an assessment of the observational evidence and possible fate. *J. Geophys. Res.* **108**. doi:10.1029/2002JE00196.

Chio, C.H., Sharma, S.K., Muenow, D.W., 2004. Raman spectroscopic studies of gypsum between 33 and 374 K. *Am. Miner.* **89**, 390–395.

Chio, C.H., Sharma, S.K., Muenow, D.W., 2005. Micro-Raman studies of hydrous ferrous sulfates and jarosites. *Spectrochim. Acta A* **61**, 2428–2433.

Chipera, S.J., Vaniman, D.T., Bish, D.L., Carey, J.W., Feldman, W.C., 2005. Experimental stability and transformation kinetics of magnesium sulfate hydrates that may be present on Mars. LPSC XXXVI, Abstract No. 1497.

Chou, I.-M., Seal II, R.R., Piatak, N., 2005. Determination of hexahydrite–starkeyite equilibria by the humidity-buffer technique at 0.1 MPa: implications for the martian H_2O cycle. GSA meeting.

Chou, I.-M., Seal II, R.R., 2003. Determination of epsomite–hexahydrite equilibria by the humidity-buffer technique at 0.1 MPa with implications for phase equilibria in the system $MgSO_4$–H_2O. *Astrobiology* **3**, 619–629.

Chou, I.-M., Seal II, R.R., Hemingway, B.S., 2002. Determination of melanterite–rozenite and chalcanthite–bonattite equilibria by humidity measurements at 0.1 MPa. *Amer. Miner.* **87**, 108–114.

Clark, B.C., Baird, A.K., Weldon, R.J., Tsusaki, D.M., Schnabel, L., Candelaria, M.P., 1982. Chemical composition of Martian fines. *J. Geophys. Res.* **87**, 10059–10067.

Clark, B.C., Richter, L., Gellert, R., Farrand, W., Ming, D., Morris, D., Yen, A., 2005. First low-iron materials on Mars and possibility of a major montmorillonite component. *AGU Abstract*, P12A-04.

Crystal Impact, 1998–2002. Copyright, GbR, Bonn, Germany.

Emons, H.H., Ziegenbalg, G., Naumann, R., Paulik, F., 1990. Thermal decomposition of the magnesium sulphate hydrates under quasi-isothermal and quasi-isobaric conditions. *J. Therm. Anal.* **36**, 1265–1279.

Feldman, W.C., Prettyman, T.H., Maurice, S., Plaut, J.J., Bish, D.L., Vaniman, D.T., Mellon, M.T., Metzger, A.E., Squyres, S.W., Karunatillake, S., Boynton, W.V., Elphic, R.C., Funsten, H.O., Lawrence, D.J., Tokar, R.L., 2004. The global distribution of near-surface hydrogen on Mars. *J. Geophys. Res.* **109** (E09006). doi:10.1029/2003JE00216.

Feldman, W.C., Prettyman, T.H., Maurice, S., Nelli, S., Elphic, R., Funsten, H.O., Gasnault, O., Lawrence, D.J., Murphy, J.R., Tokar, R.L., Vaniman, D.T., 2005. Topographic control of hydrogen deposits at low latitude to mid latitude of Mars. *J. Geophys. Res.* **110**. doi:10.1029/2005JE00245.

Gellert, R., Rieder, R., Bruckner, J., Clark, B.C., Dreibus, G., Klingelhöfer, G., Lugmair, G., Ming, D.W., Wänke, H., Yen, A., Zipfel, J., Squyres, S.W., 2006. The alpha particle X-ray spectrometer (APXS) results from Gusev Crater and calibration report. *J. Geophys. Res.* **V111**, E02S05.

Gellert, R., Rieder, R., Anderson, R.C., Brückner, J., Clark, B.C., Dreibus, G., Economou, T., Klingelhöfer, G., Lugmair, G.W., Ming, D.W., Squyres, S.W., d'Uston, C., Wänke, H., Yen, A., Zipfel, J., 2004. Chemistry of rocks and soils in Gusev Crater from the alpha particle X-ray spectrometer. *Science* **305**, 829–832.

Gendrin, A., Mangold, N., Bibring, J.-P., Langevin, Y., Gondet, B., Poulet, F., Bonnello, G., Quantin, C., Mustard, J.F., Arvidson, R.E., Mouélic, S.L., 2005. Sulfates in martian layered terrains: the OMEGA/Mars Express view. *Science* **V307**, 1587–1591 (10.1126/science.1109087).

Golden, D.C., Ming, D.W., Morris, R.V., Mertzman, S.A., 2005. Laboratory-simulated acid-sulfate weathering of basaltic materials: implications for formation of sulfates at Meridiani Planum and Gusev crater, Mars. *J. Geophys. Res.* **110**, E12S07. doi:10.1029/2005JE002451.

Greenspan, L., 1977. Humidity fixed points of binary saturated aqueous solution. *J. Res. Natl. Bureau of Standards—A. Phys. Chem.* **81A** (1), 89–96.

Haskin, L.A., Wang, A., Jolliff, B.L., Korotev, R.L., Rockow, K.M., Viskupic, K.M., 1997. Laser Raman spectroscopic determination of mineral proportions in rocks on planetary surface. Twenty-eighth Lunar and Planetary Science Conference, Part 2, pp. 523–524.

Haskin, L.A., Wang, A., Jolliff, B.L., McSween, H.Y., Clark, B.C., Des Marais, D.J., McLennan, S.M., Tosca, N.J., Hurowitz, J.A., Farmer, J.D., Yen, A., Squyres, S.W., Arvidson, R.E., Klingelhöfer, G., Schröder, C., de Souza, J., Paulo, A., Morris, R.V., Ming, D.W., Gellert, R., Zipfel, J., Brückner, J., Bell, I., James, F., Herkenhoff, K., Christensen, P.R., Ruff, S., Blaney, D., Gorevan, S., Cabrol, N.A., Crumpler, L., Grant, J., Soderblom, L., 2005. Water alteration of rocks and soils from the Spirit rover site, Gusev Crater, Mars. *Nature* **436**, 66–69.

Herman, R.G., Bogdon, C.E., Sommer, A.J., Simpson, D.R., 1987. Discrimination among carbonate minerals by Raman spectroscopy using the laser microprobe. *Appl. Spectrosc.* **41**, 437–440.

Hogenboom, D.L., Kargel, J.S., Ganasan, J.P., Lee, L., 1995. Magnesium sulfate–water to 400 MPa using a novel piezometer; densities, phase equilibria, and planetological implications. *Icarus* **115**, 258–277.

Hynek, B., Phillips, R., 2001. Evidence for extensive denudation of the Martian highlands. *Geology* **29**, 407–410.

Hynek, B., Phillips, R., 2003. New data reveal mature, integrated drainage systems on Mars indicative of past precipitation. *Geology* **31**, 757–760.

Klingelhöfer, G.R.D.S., De Souza Jr., P.A., Yen, A., Gellert, R., Evlanov, E.N., Zubkov, B., Foh, J., Bonnes, U., Kankeleit, E., Gütlich, P., Ming, D.W., Renz, F., Wdowiak, T., Squyres, S.W., Arvidson, R.E., Morris, R.V., Bernhardt, B., Schröder, C., 2004. Jarosite and hematite at Meridiani Planum from Opportunity's Mössbauer spectrometer. *Science* **306** (5702), 1740–1745, 03 DEC 2004.

Kuebler, K.E., Jolliff, B.L., Wang, A., Haskin, L.A., 2005. Extracting olivine (Fo–Fa) compositions from Raman spectral peak positions. XXXVI Lunar & Planetary Sciences Conference, Abstract No. 2068.

Kuebler, K.E., Wang, A., Abbott, K., Haskin, L.A., 2001. Can we detect carbonate and sulfate minerals on the surface of Mars by Raman spectroscopy? XXXII LPSC, Abstract No. 1889.

Kuebler, K.E., Wang, A., Haskin, L.A., Jolliff, B.L., 2003. A Study of olivine alteration to iddingsite using Raman spectroscopy. XXXIV LPSC, Abstract No. 1953.

LaFont, R., Vinh, L.D., 1966. Effect Raman d'un monocristal de sulfate de magnesoium hexahydrate. *C.R. Acad. Sci. Paris ser. B* **t.262**, 49–51.

McMillan, P., 1984. Structural studies of silicate glasses and melts—applications and limitations of Raman spectroscopy. *Amer. Miner.* **69**, 622–644.

McSween Jr., H.Y., Murchie, S.L., Crisp, J.A., Bridges, N.T., Anderson, R.C., Bell III, J.F., Britt, D.T., Brueckner, J., Dreibus, G., Economou, T., Ghosh, A., Golombek, M.P., Greenwood, J.P., Johnson, J.R., Moore, H.J., Morris, R.V., Parker, T.J., Rieder, R., Singer, R.B., Waenke, H., 1999. Chemical, multispectral, and textural constraints on the composition and origin of rocks at the Mars Pathfinder landing site. *J. Geophys. Res.* **104** (no. E4), 8679–8715 (19990425).

Ming, D.W., Mittlefehldt, D.W., Morris, R.V., Golden, D.C., Gellert, R., Yen, A., Clark, B.C., Squyres, S.W., Farrand, W.H., Ruff, S.W., Arvidson, R.A., Klingelhöfer, G., Rodionov, D.S., Schröder, C., de Souza Jr., P.A., Wang, A., 2006. Geochemical and mineralogical indicators for aqueous processes in the Columbia Hills of Gusev Crater Mars. *J. Geophys. Res.* **V111**, E02S12.

Misra, A.K., Sharma, S.K., Chi Hong Chio, Lucey, P.G., 2006. Detection of water and water bearing minerals from 10 m distance under bright condition using remote Raman system. Lunar and Planetary Science Conference, XXXVII, Abstract No. 2155.

Nakamoto, K., 1997. *Infrared and Raman Spectra of Inorganic and Coordination Compounds*, fifth ed. John Wiley & Sons, New York.

Peterson, R.C., Wang, R., 2006. Crystal moulds on Mars explained by a possible new mineral species and how incongruent melting of this hydrated magnesium sulfate could explain outwash features seen on the Martian surface. *Geology*, in press.

Rentzeperis, P.J., Soldatos, C.T., 1958. The crystal structure of the anhydrous magnesium sulphate. *Acta Cryst.* **11**, 686–688.

Rieder, R., Economou, T., Waenke, H., Turkevich, A., Crisp, J., Brueckner, J., Dreibus, G., McSween Jr., H.Y., 1997. The chemical composition of Martian soil and rocks returned by the Mobile Alpha Proton X-ray Spectrometer; preliminary results from the X-ray mode. *Science* **278** (5344 (19971205)), 1771–1774.

Rieder, R.C., Dreibus, G., Economou, T., Klingelhöfer, G., Lugmair, G.W., Ming, D.W., Squyres, S.W., D'Uston, C., Wänke, H., Yen, A., Zipfel, J., Gellert, R., Anderson, R.C., Brückner, J., 2004. Chemistry of rocks and soils at Meridiani Planum from the Alpha Particle X-ray Spectrometer. *Science* **306** (5702), 1746–1749 (03 December 2004).

Sharma, S.K., Chio, C.H., Muenow, D.W., 2006. Raman spectroscopic investigation of ferrous sulfate hydrates, Lunar and Planetary Science Conference, XXXVII, Abstract No. 2069.

Sharma, S.K., Angel, S.M., Ghosh, M., Hubble, H.W., Lucey, P.G., 2002. A remote pulsed-laser Raman spectroscopy system for mineral analysis on planetary surfaces to 66 meters. *Appl. Spectrosc.* **56**, 699–705.

Squyres, S.W., Grotzinger, J.P., Arvidson, R.E., Bell III, J.F., Calvin, W., Christensen, P.R., Clark, B.C., Crisp, J.A., Farrand, W.H., Herkenhoff, K.E., Johnson, J.R., Klingelhöfer, G., Knoll, A.H., McLennan, S.M.,

McSween, Morris, R.V., Rice Jr., J.W., Rieder, R., Soderblom, L.A., . In situ evidence for an ancient aqueous environment at Meridiani Planum, Mars. *Science* **3–6** (5702), 1709–1714.

Tosca, N.S., Mclennan, S.M., Lindsley, D., Schoonen, M., 2004. Acid-sulfate weathering of synthetic Martian basalt: the acid-fog model revisited. *J. Geophys. Res.* **109**, E05003. doi:10.1029/2003JE002218.

Vaniman, D.T., Bish, D.L., Chipera, S.J., Flalips, C.I., Carey, J.W., Feldman, W.C., 2004. Magnesium sulphate salts and the history of water on Mars. *Nature* (V431), 663–665.

Vaniman, D.T., Chipera, S.J., Bish, D.L., Carey, J.W., Feldman, W.C., 2005. Martian relevance of dehydration and rehydration in the Mg-sulfate System. XXXVI Lunars and Planetary Science Conference, Abstract No. 1486.

Walrafen, G.E., Yang, W.H., Chu, C., 2002. High-temperature Raman investigation of concentrated sulfuric acid mixtures: measurement of H-bond ΔH values between H_3O^+ or H_5O^{2+} and HSO_4^-. *J. Chem. Phys. A.* **106** (43), 10162–10173.

Walrafen, G.E., Young, T.F., 1960. Structure of oleum. *Trans. Faraday Soc.* **56**, 1419–1425.

Wang, A., Dhamelincourt, P., Turrell, G., 1988. Raman and infrared spectroscopic investigation of the cation distributions in amphiboles. *J. Mol. Struct.* **175**, 183–188.

Wang, A., Han, J., Guo, L., Yu, J., Zeng, P., 1994. A database of standard Raman spectra of mineral and related inorganic crystals. *Appl. Spectrosc.* **48**, p959–p968.

Wang, A., Haskin, A.L., Cortez, E., 1998. A Raman spectroscopic sensor for in situ mineral characterization on planetary surface. *Appl. Spectrosc.* **52**, 477–487.

Wang, A., Haskin, L.A., Korotev, R.L., Jolliff, B.L., de Souza Jr., P., Kusack, A.G., and the Athena Science Team. 2005a. Evidence of phyllosilicate in Wooly Patch— An altered rock encountered on the Spirit rover traverse. LPSC XXXVI, Abstract No. 2327.

Wang, A., Haskin, L.A., Lane, A.L., Wdowiak, T.J., Squyres, S.W., Wilson, R.J., Hovland, L.E., Manatt, k.S., Raouf, N., Smith, C.D., 2003. Development of the Mars Microbeam Raman Spectrometer (MMRS). *J. Geophys. Res.* **108** (E1). doi:10.1029/2002JE00190.

Wang, A., Haskin, L.A., Squyres, S.W., Arvidson, R., Crumpler, L., Gellert, R., Hurowitz, J., Schröder, C., Tosca, N., Herkenhoff, K., Jolliff, B.L., 2005b. Sulfate deposition in regolith exposed in trenches on the plains between the Spirit landing site and Columbia Hills in Gusev Crater, Mars. LPSC XXXVI, Abstract No. 2236.

Wang, A., Haskin, L.A., Squyres, S.W., Arvidson, R., Jolliff, B.L., Crumpler, L., Gellert, R., Schröder, C., Herkenhoff, K., Hurowitz, J., Tosca, N., Farrand, W., Anderson, R., Knudson, A.T., 2006a. Sulfate deposition in subsurface regolith in Gusev Crater, Mars. *J. Geophys. Res.* **111**, E02S17.

Wang, A., Jolliff, B., Haskin, L.A., 1995. "Raman spectroscopy as a method for mineral identification on lunar robotic exploration missions. *J. Geophys. Res.* **100**, p21189–p21199.

Wang, A., Jolliff, B.L., Haskin, L.A., 1999a. Raman spectroscopic characterization of a Martian SNC meteorite: Zagami. *J. Geophys. Res.* **104**, 8509–8519.

Wang, A., Jolliff, B.L., Haskin, L.A., 1999b. Raman spectroscopic characterization of a highly weathered basalt: igneous mineralogy, alteration products, and a microorganism. *J. Geophys. Res.* **104**, 27067–27077.

Wang, A., Jolliff, B.L., Haskin, L.A., Kuebler, K.E., Viskupic, K.M., 2001. Characterization and comparison of structural and compositional features of planetary quadrilateral pyroxenes by Raman spectroscopy. *Amer. Mineral.* **86**, p790–p806.

Wang, A., Korotev, R.L., Jolliff, B.L., Haskin, L.A., Crumpler, L., Farrand, B., Herkenhoff, K., de Souza Jr., P., Kusack, A.G., Hurowitz, J., Tosca, N.J., 2006b. Evidence of phyllosilicate in Wooly Patch, an altered rock encountered at West Spur, Columbia Hills by Spirit rover. *J. Geophys. Res.* **V111**, E02S16.

Wang, A., Kuebler, K.E., Jolliff, B.L., Haskin, L.A., 2004a. Raman spectroscopy of Fe–Ti–Cr-oxides, case study: martian meteorite EETA79001. *Amer. Miner.* **89**, 665–680.

Wang, A., Kuebler, K.E., Jolliff, B.L., Haskin, L.A., 2004b. Mineralogy of a Martian meteorite as determined by Raman spectroscopy. *J. Raman Spectrosc.* **35**, 504–514.

Wang, F., Zhang, Y.H., KLi, S.H., Wang, L.Y., Zhao, L.J., 2005. A strategy for single supersaturated droplet analysis: confocal Raman investigations on the complicated hygroscopic properties of individual $MgSO_4$ droplets on the quartz substrate. *Anal. Chem.* **77**, 7148–7155.

Wdowiak, T.J., Agresti, D.G., Mirov, S.B., 1994. A laser Raman spectrometer system suitable for incorporation into lander spacecraft. XXVI LPSC, pp. 1473–1474.

Wynn-Williams, D.D., Edwards, H.G.M., 2000. Proximal analysis of regolith habitats and protective biomolecules in situ by laser Raman spectroscopy: overview of terrestrial Antarctic habitats and Mars analogs. *Icarus* **144**, 486–503.

Young, T.F., Walrafen, G.E., 1961. Raman spectra of concentrated aqueous solutions of sulfuric acid. *Trans. Faraday Soc.* **57**, 34–39.

Zalkin, A., Ruben, H., Templeton, D.H., 1964. The crystal structure and hydrogen bonding of magnesium sulfate hexahydrate. *Acta Cryst.* **17**, 235–240.

Zangmeister, C.D., Pemberton, J.E., 2000. Raman spectroscopy and atomic force microscopy of the reaction of sulfuric acid and sodium chloride. *J. Am. Chem. Soc.* **122**, 12289–12296.